Nasal Region Contribution in 3D Face Biometrics Using Shape Analysis Framework

Hassen Drira[1], Boulbaba Ben Amor[1,2], Mohamed Daoudi[1,2], and Anuj Srivastava[3]

[1] LIFL (UMR USTL/CNRS 8022), Université de Lille 1, France
[2] Institut TELECOM/TELECOM Lille 1, France
[3] Departement of Statistics, Florida State University, Tallahassee, FL 32306, USA
{hassen.drira,boulbaba.benamor,mohamed.daoudi}@telecom-lille1.eu,
anuj@stat.fsu.edu

Abstract. The main goal of this paper is to illustrate a geometric analysis of 3D facial shapes in presence of varying facial expressions using the nose region. This approach consists of the following two main steps: *(i)* Each nasal surface is automatically denoised and preprocessed to result in an indexed collection of nasal curves. During this step one detects the tip of the nose and defines a surface distance function with that tip as the reference point. The level curves of this distance function are the desired nasal curves. *(ii)* Comparisons between noses are based on optimal deformations from one to another. This, in turn, is based on optimal deformations of the corresponding nasal curves across surfaces under an elastic metric. The experimental results, generated using a subset of FRGC v2 dataset, demonstrate the success of the proposed framework in recognizing people under different facial expressions. The recognition rates obtained here exceed those for a baseline ICP algorithm on the same dataset.

Keywords: 3D face/nose biometrics, shape analysis, automatic preprocessing.

1 Introduction and Motivations

The various tools that are called *Biometric Technologies* are simply means physiological characteristics, human body parts and their appearances, used to point-point individual human beings in the course of daily activities. The appearances of body parts, especially in imaged data, have a large variability and are influenced by their shapes, colors, illumination environment, presence of other parts, and so on. Therefore, the biometrics researchers have focused on body parts and images that try to minimize this variability within class (subjects) and maximize it across classes. *3D face* has recently emerged as a major trend in facial biometric which illustrates this idea. Since 2D (visible light) images of faces are greatly susceptible to variations in the imaging environments (camera pose, illumination patterns, etc), the researchers have argued for the need to use 3D face data, typically collected by laser scanners, for studying shapes of peoples' faces

M. Tistarelli and M.S. Nixon (Eds.): ICB 2009, LNCS 5558, pp. 357–366, 2009.

and using this shape analysis for biometrics. The output from laser scanners are minimally dependent on the external environmental factors and provide faithful measurements of shapes facial surfaces. It's the case the only remaining variability that is manifested within the same class, i.e. within the measurements of the same person, is the one introduced by changes in facial expressions. Facial expressions, such as smile, serious, fear, and anger, are prime indicators of the emotional state of a person and, thus, are important in estimating mood of a person, for example in developing intelligent ambient systems, but may have a lesser role in biometric applications. In fact, variations in facial expressions change the shapes of facial surfaces to some extent and introduce a nuisance variability that has to be accounted for in shape-based 3D face recognition. We argue that the variability introduced by facial expressions has become one of the most important issues in 3D face recognition. The other important issue is related to data collection and imperfections introduced in that process. It is difficult to obtain a pristine, continuous facial surface, or a mesh representing such a surface, with the current laser technology. One typically gets holes in the scanned data in locations of eyes, lips, and outside regions. For instance, scans of people with open mouths result in holes in the mouth region.

To handle these issues – shape variability due to facial expressions and presence of holes in mouth, we advocate the use of *nose region* for biometric analysis. At the outset the shape of the nose seems like a bad choice of feature for biometrics. Indeed, the shapes of noses seem very similar to a human observer but we will support this choice using real data and automated techniques for shape analysis. We do not assert that this framework will be sufficient for identifying human subjects across a vast population, but we argue for its role in shortlisting possible hypotheses so that a reduced hypothesis set can be evaluated using a more elaborate, multi-modal biometric system. The stability of nose data collection, the efficiency of nasal shape analysis, and the invariance of nasal shape to changes in facial expressions make it an important biometric.

The rest of this paper is organized as follows, section 2 gives a brief description of FRGC database and the preprocessing step. In section 3, we explain the differentiel-geometric framework of curves and its extension to 3D surfaces that we used to analyse 3D shapes of nasal region. Finally, in section 4, we show the experimental protocol and some preliminary results on a subset of FRGC v2 database containing expressive faces.

2 Automatic Data Preprocessing

In order to assess the recognition performance of the proposed framework, we use a subset of FRGC v2 dataset. This benchmark database [9] includes 4007 3D frontal scans for 466 subjects and is considered as a challenging database as it contains sessions with both neutral and non-neutral expressions. Moreover, the laser-based 3D scanner used in the acquisition process introduces noise in the data. In fact, some of 3D face scans suffer from missing data (holes), spikes, artefacts specially in teeth region, occlusions caused by the hair, etc. We focus in

this work on designing a complete solution for 3D face analysis and recognition using only the nose region. For that purpose, it is crucial to begin by denoising the data by removing spikes, filling holes and extract only the useful part of face and then nose from original depth image. Figure 1 shows different steps of our preprocessing solution to overcome these problems. Starting from an original range image of a face, we firstly apply a 2D median filter in order to remove spikes while preserving edges. Secondly, using a smooth 2D interpolation, we fill holes by adding points in parts where the laser has been completely absorbed (e.g. eyes, eyebrows and opend mouth). Next, we use the Delaunay triangulation to generate a triangulated mesh from the point cloud. On this mesh, we localize the nose tip, necessary for cropping the useful region of the face and nose region segmentation. For this purpose, a sphere function having center the nose tip and radius $R = 100mm$ is constructed and the part inside the sphere is keeped. Finally, a collection of geodesic level curves are extracted by locating iso-geodesic points from the reference vertex (nose tip) using the Dijkstra algorithm [2]. In order to segmentate nasal region, we consider the N first level curves. For more details about data proprocessing please refer to [1]. This algorithm has successfully processed 3971 faces in FRGC v2, which means a success rate of 99.1%. Actually, it is the nose detection step that fails more than other steps. For these faces, we have fixed manually the nose tip and so we have cleaned all the FRGC v2 faces, 99.1% automatically and 0.9% manually.

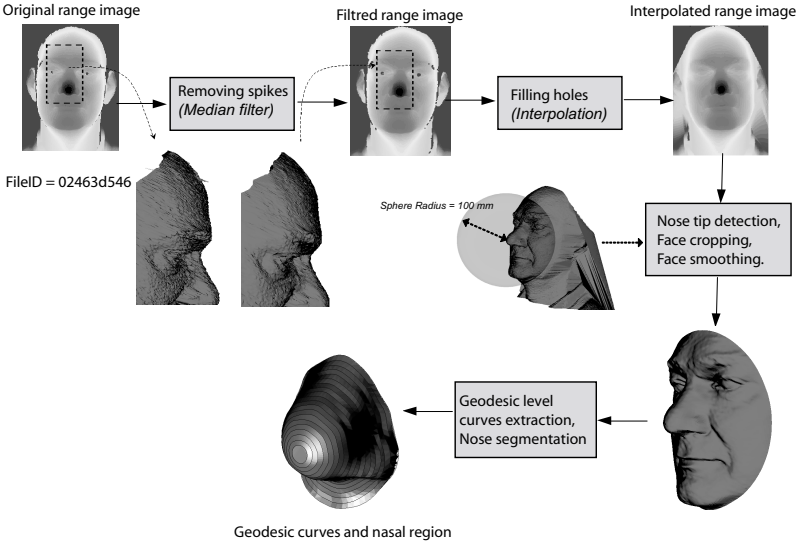

Fig. 1. Automatic FRGC data preprocessing and nose curves extraction

3 A Geometric Framework for Nose Analysis

As indicated earlier, our goal is to analyse shapes of facial surfaces using shapes of facial curves. In other words, we divide each surface into an indexed collection of simple, closed curves in $\mathbb{R}^3$ and the geometry of a surface is then studied using the geometries of the associated curves. Since these curves, previously called *facial curves*, have been defined as level curves of an intrinsic distance function on the surface, their geometries in turn are invariant to the rigid transformation (rotation and translation) of the original surface. At least theoretically, these curves jointly contain all the information about the surface and one can go back-and-forth between the surface and the curves without any ambiguity. In practice, however, some information is lost when one works with a finite subset of these curves rather than the full set. Later, through experiments on real data, we will demonstrate that the choice of facial curves for studying shapes of facial surfaces is both natural and convenient. In the following section, we will describe a differential-geometric approach for analysing shapes of simple, closed curves in $\mathbb{R}^3$. In recent years, there have been several papers for studying shapes of continuous curves. The earlier papers, including [12,6,7,8], were mainly concerned with curves in $\mathbb{R}^2$, while the curves in higher dimensions were studied later. In this paper, we will follow the theory laid out by Joshi et al. [3,4] for *elastic shape analysis* of continuous, closed curves in $\mathbb{R}^n$ and particularize it for facial curves in $\mathbb{R}^3$. The mathematical framework for using elastic shape analysis of facial curves was first presented in [11].

3.1 Nose Curves

We start by considering a closed curve β in $\mathbb{R}^3$. Since it is a closed curve, it is natural to parametrize it using $\beta : \mathbb{S}^1 \to \mathbb{R}^3$. We will assume that the parametrization is non-singular, i.e. $\|\dot{\beta}(t)\| \neq 0$ for all t. The norm used here is the Euclidean norm in $\mathbb{R}^3$. Note that the parametrization is not assumed to be arc-length; we allow a larger class of parametrizations for improved analysis. To analyse the shape of β, we shall represent it mathematically using a *square-root velocity function* (SRVF), denoted by $q(t)$, according to:

$$q(t) \doteq \frac{\dot{\beta}(t)}{\sqrt{\|\dot{\beta}(t)\|}} \ . \tag{1}$$

$q(t)$ is a special function that captures the shape of β and is particularly convenient for shape analysis, as we describe next. Firstly, the squared $\mathbb{L}^2$-norm of q, given by: $\|q\|^2 = \int_{\mathbb{S}^1} \langle q(t), q(t) \rangle \, dt = \int_{\mathbb{S}^1} \|\dot{\beta}(t)\| dt$, which is the length of β. Therefore, the $\mathbb{L}^2$-norm is convenient to analyse curves of specific lengths. Secondly, as shown in [3], the classical elastic metric for comparing shapes of curves becomes the $\mathbb{L}^2$-metric under the SRVF representation. This point is very important as it simplifies the calculus of elastic metric to the well-known calculus of functional analysis under the $\mathbb{L}^2$-metric. In order to restrict our shape analysis to closed curves, we define the set: $\mathcal{C} = \{q : \mathbb{S}^1 \to \mathbb{R}^3 | \int_{\mathbb{S}^1} q(t)\|q(t)\| dt = 0\} \subset \mathbb{L}^2(\mathbb{S}^1, \mathbb{R}^3)$.

For more details about the proposed curve shape analysis framework, reader can refer to [11]. Figure 2 shows some illustrations of this idea. The top two rows show nasal surfaces of same subject under different expressions and two level curves extracted from each of these surfaces. Between them we display geodesic paths between the corresponding level curves of the two noses, obtained using the path-straightening approach. The remaining two rows display nasal surfaces and curves of two different subjects. In each case, the first and the last curves are the ones extracted from the two surfaces, and the intermediate curves denote equally-spaced points on the corresponding geodesic α. These curves have been scaled to the same length to improve display of geodesics. We will use the notation $d(\beta_1, \beta_2)$ to denote the geodesic distance, or the length of the geodesic in $\mathcal{S}$, between the two curves β_1 and β_2.

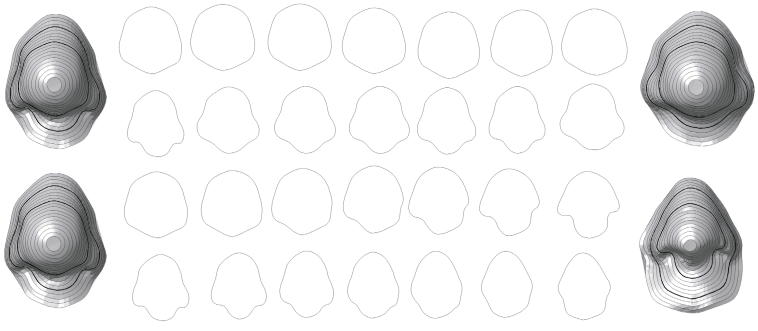

Fig. 2. Examples of geodesic between curves

Why do we expect that shapes of facial curves are central to analysing the shapes of facial surfaces? There is plenty of psychological evidence that certain facial curves, especially those around nose, lips and other prominent parts, can capture the essential features of a face. Our experiments support this idea in a mathematical way. We have computed geodesic distances between corresponding nasal curves of different faces – same people different facial expressions and different people altogether. We have found that the distances are typically smaller for faces of the same people, despite different expressions, when compared to the distances between nasal curves of different people.

3.2 Nose Surfaces

Now we extend ideas developed in the previous section for analysing shapes of nasal curves to the shapes of nose region surfaces. As mentioned earlier, we are going to represent a nose region surface S with an indexed collection of the level curves of the D function (geodesic distance from the nose tip).

That is,

$$S \leftrightarrow \{c_\lambda, \lambda \in [0, L]\} \ ,$$

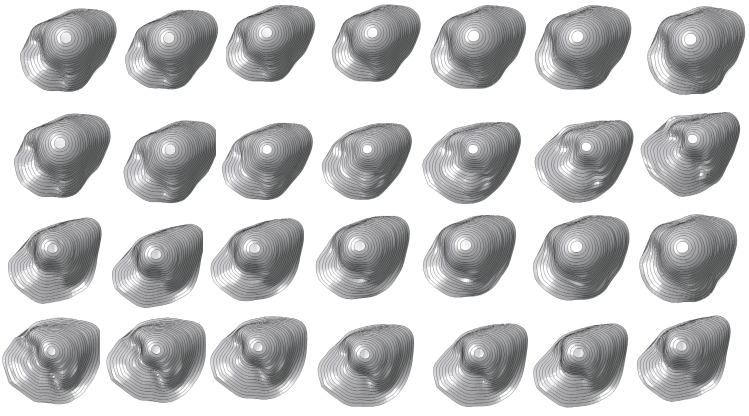

Fig. 3. Geodesic path between source and target noses (a) First row: intra-class path, source and target with different expressions (b) Three last rows: inter-class path

where c_λ is the level set associated with $D = \lambda$. Through this relation, each facial surface has been represented as an element of the set $\mathcal{C}^{[0,L]}$. In our framework, the shapes of any two noses are compared by comparing their corresponding nasal curves. Given any two surfaces S^1 and S^2, and their nasal curves $\{c^1_\lambda, \lambda \in [0, L]\}$ and $\{c^2_\lambda, \lambda \in [0, L]\}$, respectively, our idea is to compare the facial curves c^1_λ and c^2_λ, and to accumulate these differences over all λ. More formally, we define a distance: $d_s : \mathcal{C}^{[0,L]} \times \mathcal{C}^{[0,L]} \to \mathbb{R}_{\geq 0}$, given by

$$d_s(S^1, S^2) = \int_0^L d(c^1_\lambda, c^2_\lambda) d\lambda \ . \tag{2}$$

Here, the distance inside the integral is the geodesic distance function between the shapes of any curves, described in the last section. It has been shown in [10] that this distance is actually a proper distance between the elements of the $\mathcal{C}^{[0,L]}$. In addition to the distance $d_s(S^1, S^2)$, which is useful in biometry and other classification experiments, we also have a geodesic path in $\mathcal{C}^{[0,L]}$ between the two points representing by S^1 and S^2. This geodesic corresponds to the optimal elastic deformations of facial curves and, thus, facial surfaces from one to other. Shown in Figure 3 are examples of such geodesic paths between given facial surfaces – One example (top row) involves faces of same people but with different facial expressions while the other examples show geodesics between faces that belong to different people.

4 Experiments and Evaluations

we focus in our experiments on the common biometric scenarions which are authentication (or verification) and identification (or recognition). As far as verification scenarion is concerned, performance is reported on a *Receiver Operator*

Characteristic (ROC) that shows the trade-off between verification and false accept rates. In the identification scenarion, however, the results for facial identification are often displayed using a *Cumulative Match Characteristic* (CMC) curve. This curve displays the cumulative identification rates as a function of the rank distribution. This provides an indication of how close one may be to getting the correct match if the rank-one match was incorrect. In order to produce results for both scenarions and to explore effect of the presence of facial expressions on performance, a similarity matrix between a gallery and a probe datasets is computed. The gallery contains 125 sessions for 125 different subjects acquired with neutral expressions selected from FRGC v2 dataset. The probe dataset includes completely different sessions of these subjects under non-neutral facial expressions. Due to sensitivity of our algorithm (on full face) to opened mouth, expressions in probe dataset include only scans with closed mouths. In this matrix, the diagonal terms represent match scores (or *Genuine Access*) contrary to non-diagonal terms which represent Non-match scores (or *Imposter Access*). These scores allow us to produce the ROC and the CMC curves for this protocol. We compare results of our algorithm with a standard implementation of ICP which is considered as a baseline in 3D face recognition. Baseline performance serves to demonstrate that a challenge problem can be executed, to provide a minimum level of performance, and to provide a set of controls for detailed studies. The same protocol was followed to compute similarity matrices for both algorithms on the same preprocessed data.

Figure 4 shows ROC curves for our approach on face, on nose region and ICP algorithm on nose and on face. As shown in this figure, the ROC curves (for face

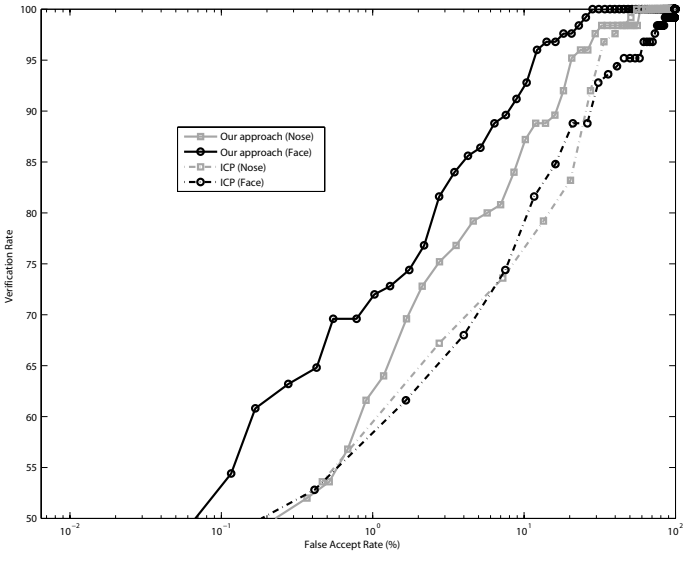

Fig. 4. ROC curves for our approach and ICP (baseline) on face and nose surfaces

and nose region) of our approach are almost always above the ICP ones. Which means that our verification rates at each false accept rate are greater than ICP ones. This result is expected as our approach is more robust in presence of facial expressions. As far as ICP is concerned, ROC curves for face and nose region are overlapped. ROC curve of our approach applied only on nose region is often above ICP ROC curves, applied on nose region and on the full face. Therefore, using only nose region in our approach gave a better verification results than ICP applied on the full face. Although, using the full face with our approach give always the better verification results.

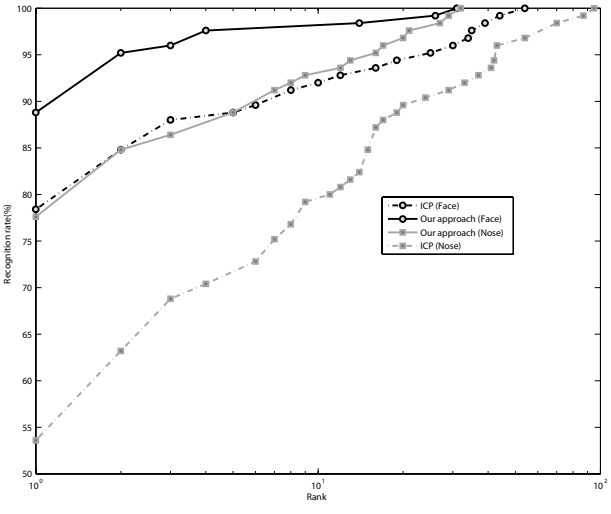

Fig. 5. CMC curves for our approach and ICP (baseline) on face and nose surfaces

These observations are also confirmed with identification scenarion which is illustrated with CMC curves of the two algorithms applied on nose region and on the full face. As shown in Figure 5, rank-one recognition rate given by our algorithm applied on the full face is the best one, it's about 88.8%. Then results of rank-one recognition for our approach applied on nose region and ICP applied on the full face are similar, about 78%. The worst result is given by ICP applied on nose region. At the rank-four, our approach on the full face is able to recognize 97.8% of the subjects in contrast with ICP on the full face which gives a similar result with our approach on the nose region, it's about 89%. After this rank, the recognition rates given by our approach on the nose region are always better than the ones given by ICP applied on the full face. So, using the full face for our approach gives always the best recognition and authentification results. However, appling our approach only on the nose region gives better results than ICP applied on the full face. Figure 6 shows some examlpes of some noses (with their faces) which are recognized by our approach but not by the baseline (ICP). This result can be explicated by the nature of the approaches themselves. Actually,

as known, ICP algorithm search for the best rigid transformations to apply on a 3D points cloud (which represents the first face or nose) to be the closest to the second 3D points cloud (the second face or nose). As shown in this figure, 3D points positions have widely changed and it is different to ICP to find a smallest rigid transformation between these noses in probe and their correspondant in gallery. Although our approach succes to recognize them as it is based on shape analysis which is more robust to facial deformations in comparison with ICP.

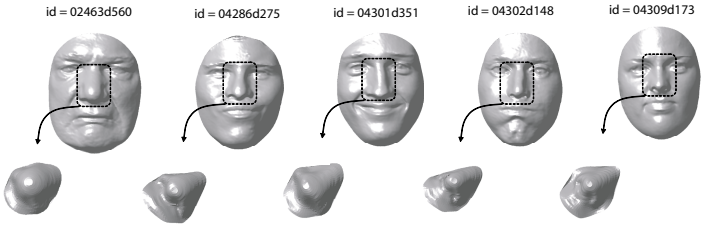

Fig. 6. Examples of noses that are recognized by our approach and not by ICP

5 Conclusions

In this paper, we have illustrated a geometric analysis of 3D nasal shapes in presence of both neutral and non-neutral facial expressions. In this analysis, the preprocessing is completely automated - the algorithm processes the face scan data, detects the tip of the nose, extracts a set of facial curves and extract nasal surface. The main tool presented in this paper is the construction of geodesic paths between arbitrary two nasal surfaces. The length of a geodesic between any two noses is computed as the geodesic length between a set of their nasal curves. This length quantifies differences in their shapes ; it also provides an optimal deformation from one to the other. In order to validate our approach in presence of facial expressions, a similarity matrix between 125 probe images with facial expressions and 125 gallery images with the neutral expression is computed. Authentication and recognition scores are produced and compared with a standard implementation of ICP as a baseline. The results of our algorithm outperform the baseline ICP algorithm which prove robustness of the proposed framework to deformations caused by facial expressions.

Acknowledgements

This research is supported in part by the ANR under the project ANR-07-SESU-004 and the Contrat de Projet Etat-Rgion (CPER) Rgion Nord-Pas-De calais Ambient Intelligence and partially supported by the following grants : ARO W911NF-04-01-0268 and AFOSR FA9550-06-1-0324 to Anuj Srivastava. Additionally, Anuj Srivastava was supported by visiting professorships from University of Lille I in summers of 2007 and 2008.

References

1. Ben Amor, B., Drira, H., Ballihi, L., Srivastava, A., Daoudi, M.: An experimental illustration of 3D facial shape analysis under facial expressions. Annals of telecommunications (accepted for publication)
2. Dijkstra, E.W.: A note on two problems in connection with graphs. Numerische Math. 1, 269–271 (1959)
3. Joshi, S.H., Klassen, E., Srivastava, A., Jermyn, I.H.: A novel representation for efficient computation of geodesics between n-dimensional curves. In: IEEE CVPR (2007)
4. Joshi, S.H., Klassen, E., Srivastava, A., Jermyn, I.H.: Removing shape-preserving transformations in square-root elastic (SRE) framework for shape analysis of curves. In: Yuille, A.L., Zhu, S.-C., Cremers, D., Wang, Y. (eds.) EMMCVPR 2007. LNCS, vol. 4679, pp. 387–398. Springer, Heidelberg (2007)
5. Klassen, E., Srivastava, A.: Geodesics between 3D closed curves using path-straightening. In: Leonardis, A., Bischof, H., Pinz, A. (eds.) ECCV 2006. LNCS, vol. 3951, pp. 95–106. Springer, Heidelberg (2006)
6. Klassen, E., Srivastava, A., Mio, W., Joshi, S.: Analysis of planar shapes using geodesic paths on shape spaces. IEEE Pattern Analysis and Machine Intelligence 26(3), 372–383 (2004)
7. Michor, P.W., Mumford, D.: Riemannian geometries on spaces of plane curves. Journal of the European Mathematical Society 88, 1–48 (2006)
8. Mio, W., Srivastava, A., Joshi, S.: On shape of plane elastic curves. International Journal of Computer Vision 73(3), 307–324 (2007)
9. Phillips, P.J., Flynn, P.J., Scruggs, T., Bowyer, K.W., Chang, J., Hoffman, K., Marques, J., Min, J., Worek, W.: Overview of the face recognition grand challenge. In: CVPR 2005: Proceedings of the 2005 IEEE Computer Society Conference on Computer Vision and Pattern Recognition (CVPR 2005), vol. 1, pp. 947–954 (2005)
10. Samir, C., Srivastava, A., Daoudi, M., Klassen, E.: An intrinsic framework for analysis of facial surfaces. International Journal of Computer Vision (accepted for publication)
11. Srivastava, A., Samir, C., Joshi, S., Daoudi, M.: Elastic shape models for face analysis using curvilinear coordinates. Journal of Mathematical Imaging and Vision (2008) (accepted for publication)
12. Younes, L.: Computable elastic distance between shapes. SIAM Journal of Applied Mathematics 58, 565–586 (1998)